Journal of Catalysis **188,** 1–13 (1999)
Article ID jcat.1999.2579, available online at http://www.idealibrary.com on IDEAL®

# Carbon Monoxide Hydrogenation on Co–Rh/$Nb_2O_5$ Catalysts

A. Frydman,*,†,[1] D. G. Castner,‡ C. T. Campbell,† and M. Schmal*,[2]

*NUCAT/PEQ/COPPE, Universidade Federal do Rio de Janeiro, CP 68502, CEP 21945, Ilha do Fundão, Rio de Janeiro, Brasil; †Department of Chemistry, University of Washington, Seattle, Washington 98195-1700; and ‡Department of Chemical Engineering, University of Washington, Seattle, Washington 98195-1750

Received September 22, 1998; revised May 28, 1999; accepted May 28, 1999

**Carbon monoxide hydrogenation activities and product distributions were investigated here for the first time on a series of seven Co–Rh/$Nb_2O_5$ catalysts: two monometallics Co and Rh supported on $Nb_2O_5$ and five bimetallics Co–Rh supported on $Nb_2O_5$ with similar Co (∼1.9 wt%) and variable Rh loadings (0.3–2.3 wt%). Catalytic performances at atmospheric pressure and 493 K were evaluated after low temperature reduction (LTR, 533–573 K) and after high temperature reduction (HTR, 773 K). Temperature-programmed reduction characterization revealed that the reduction temperature of the dominant Co phase on calcined catalysts, $Co_3O_4$, strongly decreased as the Rh/Co bulk atomic ratio increased, while the reduction temperature of the $Rh_2O_3$ phase (363 to 419 K) was not strongly influenced by the presence of $Co_3O_4$. It was observed that the activity decay effect caused by metal–support interaction was remarkably inhibited on the bimetallics with respect to the monometallics by comparing reaction rates after LTR and after HTR. The addition of Rh to the Co monometallic catalyst significantly altered the product distribution. An unusual promotion of the selectivity to long chain hydrocarbons was observed. This promotion was more intense after HTR on the bimetallic catalysts, reaching ∼56% in the diesel fraction on the bimetallic catalyst with higher Rh concentration. Alcohol selectivity was enhanced up to 3.5 and 5.4% for ethanol and propanol, respectively, on the bimetallic catalyst with lower Rh concentration. The total CO hydrogenation reaction rate and the selectivity for methane were approximately constant as the Rh concentration on the bimetallics increased, suggesting that the metal surface area did not vary considerably on these catalysts. This agrees with hydrogen adsorption measurements on the bimetallic catalysts and with the XPS surface structural characterization of the calcined Co–Rh/$Nb_2O_5$ catalysts, which revealed that the specific surface area of active metal (Rh + Co) precursor oxide did not vary considerably as the Rh concentration increased.** 

## 1. INTRODUCTION

The intrinsic properties of transition metals or group VIII elements determine part of the basis for mechanistic theories and design of CO hydrogenation catalysts. Under typical reaction temperatures (473–573 K) Fe, Ru, and Co dissociate CO to create $CH_x$ species suitable for higher hydrocarbon formation. This behavior will not be as predominant on well-known hydrogenation metals such as Ni, Cu, Pd, Pt, Ir, and Rh because the CO molecule will not dissociate as easily. In theory, this latter series of metals should be appropriate for oxygenate formation and have recently been the focus of intensive research to develop alternate routes of producing fuel additives and chemical feedstocks.

Rhodium exhibits a versatile product distribution for CO hydrogenation since it may or may not dissociate CO under reaction conditions (e.g., by changing the nature of the support material) (1, 2). Even though the CO hydrogenation reaction has been studied since the 1920s, the interest in Rh catalysts only began in 1975 when it showed efficient formation of $C_2$ oxygenates (ethanol, acetaldehyde, and acetic acid), but poor selectivity toward higher oxygenates (3–7). Ichikawa *et al.* (8–11) observed that Rh catalyst selectivity to oxygenates depends upon the type of support material, the catalyst pretreatment, the reaction conditions, the promoter effect, and the Rh precursor used. Apparently, the selectivity to oxygenates on group VIII metals is low because of the difficulty in suppressing the hydrogenative function characteristic of these metals. Cobalt-based catalysts were among the first to produce hydrocarbons from CO hydrogenation due to their ability to hydrogenate dissociated carbon species and promote chain growth (12). Co is a typical metal that adsorbs CO molecules dissociatively and so it is an appropriate catalyst for the formation of long chain hydrocarbons. Therefore, there is no surprise that only a few researchers have investigated oxygenate synthesis on Co catalysts (13–17).

Bimetallic catalysts may be considered essential to many industrial catalytic processes because of advantages such as improved stability and reducibility, slower deactivation, and noticeable increase in catalytic activity and selectivity in comparison to the monometallic constituents (18, 19). Cobalt has been used as a promoter for higher oxygenate synthesis, especially on known methanol synthesis catalysts such as ZnO–$CrO_2$, Cu/ZnO, and Cu/$Al_2O_3$ (7, 20–23). Bimetallic Co-noble metal catalysts supported on

[1] Current address: Cryofuel Systems Group, University of Victoria, P.O. Box 3055, Victoria, BC V8W 3P6, Canada.

[2] To whom correspondence should be addressed.



0021-9517/99 $30.00

different materials that have been proposed for oxygenate formation include Co–Ir/$SiO_2$ (24), Co–Ir/$Al_2O_3$ (25), Co–Pt/$Al_2O_3$ (26), Co–Ru/$SiO_2$ (27), Co–Pd/NaY (28), and Co–Rh/$TiO_2$ (29). There is general agreement that the noble metal or the bimetallic sites are primarily responsible for oxygenate formation on these catalysts. In addition, there is very little evidence to support the assumption that Co alone could produce $C_{2+}$ oxygenates by forming C–C or C–O bonds (30).

In principle, the addition of a second metal allows changes in the electronic structure, arrangement, and size of atom clusters and in the adsorption properties (19). This is beneficial to the CO hydrogenation reaction in particular because carbon chain growth would progress more efficiently on large atom clusters. These positive features of the bimetallic catalysts have been described as *synergistic effects* by several authors. For instance, Co–Ru bimetallic interactions were found to increase reaction rate and selectivity toward $C_{5+}$ hydrocarbons in CO hydrogenation and to improve catalyst regeneration (31–36), reducibility (37–40), and alcohol synthesis (41). It is claimed that Co properties in the CO hydrogenation reaction are complemented by adding a second metal, typically noble, to lower the reduction temperature and promote better regenerability, both very attractive features for commercial applications. It is suggested that the noble metal behaves as spillover source and storage for hydrogen atoms at lower temperatures, which influences not only reduction processes but also the removal of carbon deposits formed during the reaction (42). There have been a few studies on Co–Rh catalysts (29, 30, 43–45). These are promising candidates for improved oxygenate selectivities from the $CO/H_2$ reaction because of the combination of Co's ability in promoting carbon chain growth with Rh's versatility in adsorbing CO molecules in either molecular or dissociate forms (2, 46).

Niobium pentoxide as a support material for CO hydrogenation metal catalysts was the subject of a few studies (47–53). These studies have reported that the use of $Nb_2O_5$ as a support results in better CO hydrogenation activities for Rh/$Nb_2O_5$ in comparison to Rh supported on $ZrO_2$, $Al_2O_3$, $SiO_2$, or MgO (51) and for Ni/$Nb_2O_5$ in comparison to Ni/$SiO_2$ (52). Enhanced selectivity for high-molecular-weight hydrocarbons in CO hydrogenation over Co/$Nb_2O_5$ (47, 48) and Ni/$Nb_2O_5$ (53) compared to more traditional supports, such as $Al_2O_3$ (47, 48, 53) and $SiO_2$ (47), was also observed.

In this study, for the first time, a series Co–Rh/$Nb_2O_5$ catalysts is investigated with respect to their performance in the CO hydrogenation reaction as an attempt to improve the $C_{2+}$ alcohol selectivity of Co-based catalysts. To this date, there are no catalytic data for Co–Rh/$Nb_2O_5$ catalysts and characterization has not been presented until recently (54). TPR characterization of these catalysts is discussed and correlated with the XPS characterization results reported elsewhere (54).

## 2. EXPERIMENTAL

### 2.1. Catalyst Preparation

The support material obtained from CBMM (Companhia Brasileira de Metalurgia e Mineração) was originally niobic acid AD399 (99.8% purity). After calcination at 873 K for 4 h, niobic acid is converted from an amorphous phase to the crystalline TT or T form of niobium pentoxide (55). Under these conditions, $Nb_2O_5$ is a macroporous material. The catalysts were prepared by incipient wetness impregnation and the bimetallics by coimpregnation. The Co and Rh precursors were, respectively, $Co(NO_3)_2 \cdot 6H_2O$ (Riedel-de Häen, 99% purity) and $Rh(NO_3)_3$ (Aldrich, solution in 10–15% $HNO_3$, 10% Rh content). The Co content was kept approximately constant (ca. 1.9 wt%) and the Rh/Co bulk atomic ratio for the bimetallic catalysts varied approximately from 0.09 to 0.72. The atomic ratio is used to label the catalysts (e.g., the highest Rh/Co ratio catalyst is referred to as the "Co72Rh/Nb"). After impregnation, all catalysts were dried overnight at 383 K, followed by calcination at 673 K for 4 h, and stored for characterization and catalytic test. Table 1 shows the bulk Co and Rh concentrations determined by atomic absorption and the $N_2$ BET surface areas of the support material and the catalysts.

### 2.2. TPR

The stoichiometry of the supported oxides and the interactions between these phases and the support material were studied in a custom-made temperature-programmed reduction (TPR) apparatus by flowing a reduction gas mixture of 1.75% $H_2$ in argon (30 ml/min) over the sample and ramping the temperature up at a constant rate (8 K/min) from 298 to 1373 K for each experiment. The $H_2$ consumption was measured with a thermal conductivity detector. Before it reached the detector, the reacted gas mixture was

**TABLE 1**

**Characterization of Support Material and Co–Rh/$Nb_2O_5$ Catalysts**

| | BET area ($m^2$/g) | Co (wt%) | Rh (wt%) |
|---|---|---|---|
| Support material | | | |
| Niobic acid | 95 | | |
| $Nb_2O_5$ | 25 | | |
| Catalysts | | | |
| Co/Nb | 29 | 1.9 | — |
| Rh/Nb | 29 | — | 0.85 |
| Co09Rh/Nb | 22 | 2.0 | 0.31 |
| Co19Rh/Nb | 26 | 1.85 | 0.60 |
| Co24Rh/Nb | 22 | 1.75 | 0.73 |
| Co72Rh/Nb | 20 | 1.85 | 2.33 |

*Note.* Reference compounds $Co_3O_4$ and $Rh_2O_3$ for TPR analysis were also prepared. The $Co_3O_4$ sample was obtained by calcination of the cobalt nitrate precursor at 673 K for 4 h. The rhodium nitrate precursor was carefully evaporated overnight at 323 K and the residue was calcined at 673 K for 4 h to obtain the $Rh_2O_3$ sample.

filtered by molecular sieve to remove the water produced in the reduction. Before the TPR experiment, the sample was dried overnight at 383 K. A mass of ∼0.5 g of each sample was used in the analysis except for the Co72Rh/Nb sample (∼0.2 g).

### 2.3. Continuous-Flow Hydrogen Adsorption

The TPR apparatus was also used to perform continuous-flow $H_2$ adsorption measurements at room temperature (∼298 K) using the same 1.75% $H_2$/Ar mixture. Total and reversible amounts of hydrogen were measured. The irreversible hydrogen adsorbed was determined after subtracting the void volume. Samples measured were Rh/Nb and two bimetallics (Co09Rh/Nb and Co72Rh/Nb).

### 2.4. CO Hydrogenation

Catalytic evaluation of the Co–Rh/$Nb_2O_5$ samples with the CO hydrogenation reaction was performed on a small-scale stainless steel unit. Operational conditions and procedures were selected based on the results from previous studies (48–50). Gases used were $H_2$ (commercial grade, for sample reduction), $N_2$ (commercial grade, for reactor purge), 5% $O_2/N_2$ mixture (for sample reoxidation), and 31.7% CO/64.3% $H_2$/4% He (feed gas for reaction). Helium was used as an internal standard to calculate the total CO conversions, as explained below. A set of valves was used to select the required gases. These gases were passed through the following filtering elements (at room temperature, ∼293 K): a Pd-based catalyst to remove residual $O_2$ and a molecular sieve to remove water traces. The 5% $O_2/N_2$ mixture went through the molecular sieve filter only. In addition, the mixture CO/$H_2$/He passed through an activated carbon filter (heated at 353 K) to remove any Fe carbonyl compounds formed in the gas bottle.

The fixed-bed reactor was a vertical stainless steel tube approximately 1.5 cm in i.d. with a wall thickness of 2 mm and a length of 15 cm. A stainless steel screen was placed 5 cm from the bottom of the reactor to hold the catalyst sample. The gas flow went from bottom to top. A type J thermocouple, used to monitor reaction temperature, was inserted into a 3.18-mm (1/8″)-diameter tube welded to the wall of the reactor at 2 cm above the screen. The thermocouple tip reached the center of the reactor. The reactor was enclosed by a ceramic oven equipped with another type J thermocouple connected to a temperature programmer and controller. A mass of sample between 0.7 and 2 g was dried overnight at 383 K. The sample was then placed in the reactor for reduction. Nitrogen passed through the sample for ∼5–10 min to purge air from the reactor. Hydrogen flow for catalyst reduction was 20 ml/min. The oven temperature programmer was set to heat from room temperature to the chosen reduction temperature (533, 573, or 773 K) at a slow rate of 2 K/min. The final temperature was maintained for 2 or 16 h. Immediately after the reduction, the reactor was purged with $N_2$ at the reduction temperature for ∼5–10 min and then cooled down under $N_2$ flow to the reaction temperature (493 K). The reaction was started after the temperature had stabilized by flowing the CO/$H_2$/He mixture into the reactor at a rate of 10–20 ml/min to ensure constant space velocity for all experiments. The total reaction time was approximately 24 h.

Reaction products were analyzed on line with two gas chromatographs placed in series: first a VARIAN-3700 equipped with a flame ionization detector and then a CG-25 equipped with a thermal conductivity detector. A Megabore HP-1 column was installed on the VARIAN-3700 (methyl silicone; 0.53 mm in diameter; 30 m in length; oven operated from 273 to 503 K at 8 K/min for each analysis; initial temperature was kept constant for 3 min). The CG-25 had a Porapak Q packed column, 3.18 mm (1/8”) in diameter and 2 m long (oven operated at constant temperature, 383 K). The carrier gas on both chromatographs was $H_2$ flowing at 20 ml/min. After the reactor, the tubing lines were kept at ∼503 K to avoid product condensation. This hot stream passed through a six-way injection valve that collected ∼0.1 $cm^3$ of gas sample to be injected first in the Megabore column for hydrocarbon (from $C_1$ to $C_{30}$), olefin, and alcohol analysis (∼2.5 h each injection). After the six-way valve, the gas product passed through a trap heated at 353 K to collect residue of condensable products. After this trap, the remaining products were mainly unreacted CO, He, $CO_2$, light hydrocarbons from $C_1$ to $C_4$, and water, which were injected in the Porapak Q column (∼20 min each injection). Product identification was based on previous studies (49, 50), injection of chromatographic standards, and comparison to similar columns (56, 57). Response factors were taken from the literature (58). After each run on the Megabore column, a blank sample (carrier gas only) was injected with identical temperature programming to purge the heavy products from the column before the next actual injection. Table 2 presents the conditions of the catalytic tests.

## 3. RESULTS AND DISCUSSION

### 3.1. TPR

Figure 1 shows the reduction profiles of the series of Co–Rh/$Nb_2O_5$ catalysts. The main Co and Rh oxide phases after calcination of the respective nitrate precursors correspond to $Co_3O_4$ and $Rh_2O_3$, as suggested by TPR lineshapes of the samples compared to the TPR of the reference compounds $Co_3O_4$ and $Rh_2O_3$. Indeed, these two forms are the most stable oxidation states of the pure elements under our calcination conditions (59). XPS analysis of these samples (54) revealed that bulk-like $Co_3O_4$ is the main Co phase present on the surface of the calcined catalyst particles (weight fraction between 78 and 90%), with the remainder in a $Co^{2+}$ surface adsorbed phase on the $Nb_2O_5$. It is known that $Co_3O_4$

**TABLE 2**

**CO Hydrogenation Reaction Conditions ($H_2/CO = 2$) at 0.1 MPa and 493 K**

| Catalyst | Mass (g) | $T_{reduction}$ (K) | $Flow_{feed}$ (ml/min) |
|---|---|---|---|
| Co/Nb (LTR) | 1 | 573 | 20 |
| Co/Nb (HTR) | 2 | 773 | 10.5 |
| Co09Rh/Nb (LTR) | 1 | 533 | 20 |
| Co09Rh/Nb (HTR) | 1 | 773 | 20 |
| Co19Rh/Nb (LTR) | 1 | 533 | 20 |
| Co19Rh/Nb (HTR) | 1 | 773 | 20 |
| Co24Rh/Nb (LTR) | 1 | 533 | 20 |
| Co24Rh/Nb (HTR) | 1 | 773 | 20 |
| Co72Rh/Nb (LTR) | 1 | 533 | 20 |
| Co72Rh/Nb (HTR) | 1 | 773 | 20 |
| Rh/Nb (LTR) | 0.7 | 573 | 20 |
| Rh/Nb (HTR) | 1 | 773 | 20 |

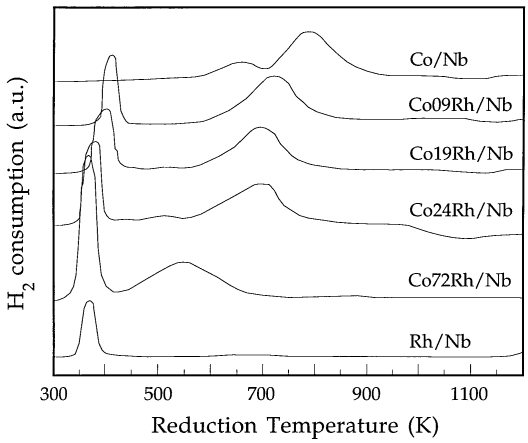


**FIG. 1.** Temperature-programmed reduction (TPR) profiles of Co–$Rh/Nb_2O_5$ catalysts.

reduces in two steps (43, 60–63): $Co_3O_4$ to CoO and CoO to $Co^0$. The stoichiometries of the first and second steps of $Co_3O_4$ reduction determine ideal consumptions of 0.33 and 1.00 $H_2$ molecules per Co atom, respectively. $Rh_2O_3$ normally reduces in one single step (43): $Rh_2O_3$ to $Rh^0$, resulting in a stoichiometric consumption of 1.50 $H_2$ molecules per Rh atom.

The hydrogen consumption determined from TPR analysis of the Co–$Rh/Nb_2O_5$ catalysts is shown in Table 3. The TPR profiles of Fig. 1 show two main regions of hydrogen consumption: Region I for temperatures below 410 K and Region II for temperatures between 410 and 950 K. Based on literature data (43, 60–63), it is assumed that the reduction of $Rh_2O_3$ to $Rh^0$ occurs in Region I and the reduction of $Co_3O_4$ to CoO and then to $Co^0$ occurs primarily in Region II.

The TPR spectra of the Co/Nb catalyst (Fig. 1) exhibited two peaks of hydrogen consumption at 655 and 787 K (Region II) consistent with the two reduction steps of $Co_3O_4$ noted above. This is a well known result for Co/$Nb_2O_5$ (48, 49), Co/$Al_2O_3$ (60), and Co/$TiO_2$ (43). By comparing the reduction profile of the Co/Nb catalyst to the reduction profiles of physical mixtures of $Co_3O_4 + Nb_2O_5$ and $CoO + Nb_2O_5$ (50), it was observed that the reduction lineshape for the Co/Nb catalyst closely resembled the one obtained for the physical mixture of $Co_3O_4 + Nb_2O_5$, suggesting that the predominant Co species on the calcined Co/Nb catalyst is $Co_3O_4$. (XPS characterization of this sample has demonstrated that 90 wt% of the Co on the surface is present in form of bulk-like $Co_3O_4$ (54).) An excess of 0.32 moles of $H_2$ were consumed per mole of Co ($H_2$/Co) in the TPR of the Co/Nb catalyst, compared to that expected for the stoichiometry of reduction of $Co_3O_4$ to $Co^0$ (Table 3). If the two peaks in the TPR profile of Co/Nb are resolved separately, it turns out that the excess is consumed in the second peak (higher temperature), where CoO is

**TABLE 3**

**Hydrogen Consumption in the TPR Analysis of Co–$Rh/Nb_2O_5$ Catalysts**

| | No. of moles ($\times 10^6$) | | No. of moles of $H_2$ consumed ($\times 10^4$) | | | | | $H_2$ in excess[c] | |
|---|---|---|---|---|---|---|---|---|---|
| | | | Ideal[a] | | | In the TPR[b] | | | |
| Sample | Rh | Co | CoO | $Co_3O_4$ | $Rh_2O_3$ | Reg. I | Reg. II | $H_2/g_{cat}$ ($\times 10^4$) | $H/cm^2$ ($\times 10^{-14}$) |
| Co/Nb | — | 163 | 1.63 | 0.54 | — | — | 2.69 | 1.03 | 2.12 |
| Co09Rh/Nb | 15 | 172 | 1.72 | 0.57 | 0.23 | 0.71 | 2.32 | 1.02 | 2.85 |
| Co19Rh/Nb | 29 | 159 | 1.59 | 0.52 | 0.44 | 0.92 | 2.15 | 1.03 | 2.33 |
| Co24Rh/Nb | 35 | 148 | 1.48 | 0.49 | 0.53 | 1.02 | 1.99 | 1.02 | 2.92 |
| Co72Rh/Nb | 46 | 64 | 0.64 | 0.21 | 0.69 | 0.73 | 0.98 | 0.35 | 2.54 |
| Rh/Nb | 43 | — | — | — | 0.65 | 0.66 | — | 0.03 | 0.04 |

[a] Number of $H_2$ moles consumed according to the stoichiometry of reduction of $Co_3O_4$ to CoO, CoO to $Co^0$, and $Rh_2O_3$ to $Rh^0$, respectively.

[b] Number of $H_2$ moles consumed in regions I and II of the TPR profiles of Fig. 1.

[c] Total $H_2$ consumed in excess of that expected from $Co_3O_4$ and $Rh_2O_3$ alone as moles $H_2$ per mass of sample and as the number of H atoms per $cm^2$ of support material, respectively.

reduced to $Co^0$ and species originating from the support material are reduced as well ($Nb_2O_5$ is reducible starting at temperatures around 623 K (64)). This excess has also been observed by Silva *et al.* (48), however at a lower level ($H_2/Co = 0.16$), for a 5% Co/$Nb_2O_5$ catalyst of similar BET surface area and prepared by the same procedure. In that case, the higher Co content (5%) resulted in larger $Co_3O_4$ particles after calcination (~26 nm according to XRD data (48)). On the other hand, our calcined Co/Nb catalyst, with the Co content of 2%, had smaller $Co_3O_4$ particles (~9 nm from XPS modeling analysis (54)). Thus, the Co particle size seems to have an effect when comparing on a $H_2$/Co basis. However, the amounts of excess $H_2$ consumed in these two studies were similar when compared on a H per unit area basis. An excess of hydrogen consumed in the TPR at higher temperatures may also result from partial reduction of the support material, as suggested elsewhere (48). The amount of reduction of the support could easily scale with its BET area, if kinetically controlled.

Soares (65) and Noronha (66) have also used TPR to characterize a 2% Co/$Nb_2O_5$ catalyst with a BET surface area of 50 $m^2/g$ (twice the one of the present study) and found the $H_2/Co = 1.00$ (lower by 0.33 than that needed to reduce $Co_3O_4$ to $Co^0$). Noronha (66) has determined by magnetic measurements that 50–60 wt% of the Co on a 2% Co/$Nb_2O_5$ calcined catalyst was reduced to $Co^0$ following reduction at 773 K and that the remainder Co was in the form of $Co^{2+}$. Our XPS analysis revealed the presence of a $Co^{2+}$ species in all Co-containing catalysts that was ~1 monolayer thick (~0.3 nm) and covered ~5–12% of the support surface (54). Our Co/Nb calcined catalyst had only 10 wt% of the total Co in the form of these $Co^{2+}$ species (54). For such low Co content catalysts (~2%), this suggests that the higher the BET surface area is the higher the amount of well-dispersed, difficult to reduce $Co^{2+}$ species formed after calcination, which may account for the lower hydrogen consumption in the TPR of Noronha (66).

The reduction profile of the calcined Rh/Nb catalyst (Fig. 1) presented one single peak at 367 K. Reduction in one step is consistent with results obtained for Rh/$Al_2O_3$ (43) and suggests that $Rh_2O_3$ is the predominant form of Rh after calcination (pure $Rh_2O_3$ reduces at 408 K (43)). In addition, the hydrogen consumption (Table 3) is the same, within experimental error, as the amount expected from the stoichiometry of the reduction of $Rh_2O_3$ to $Rh^0$.

The TPR spectra of the bimetallic samples (Fig. 1) strongly suggested $Co_3O_4$ and $Rh_2O_3$ were the predominant oxide forms of Co and Rh, respectively, on the calcined catalysts. Theses two forms have also been suggested as the main oxide forms in other Co–Rh catalysts supported on $Al_2O_3$ and $TiO_2$ (43). In addition, the lineshapes of the bimetallic samples suggested an intimate contact between cobalt and rhodium phases after the calcination treatment, since their reduction profiles are not just a superposition of the monometallic profiles. Specifically, the $Co_3O_4$ in the bimetallic catalysts was reduced at substantially lower temperatures when Rh was present, and only one high temperature reduction peak was observed. The reduction temperature of this peak decreased with increasing Rh content of the bimetallic catalysts (see Fig. 2). This shows that the presence of Rh strongly influences the reduction of Co oxide. This is consistent with the expected behavior for

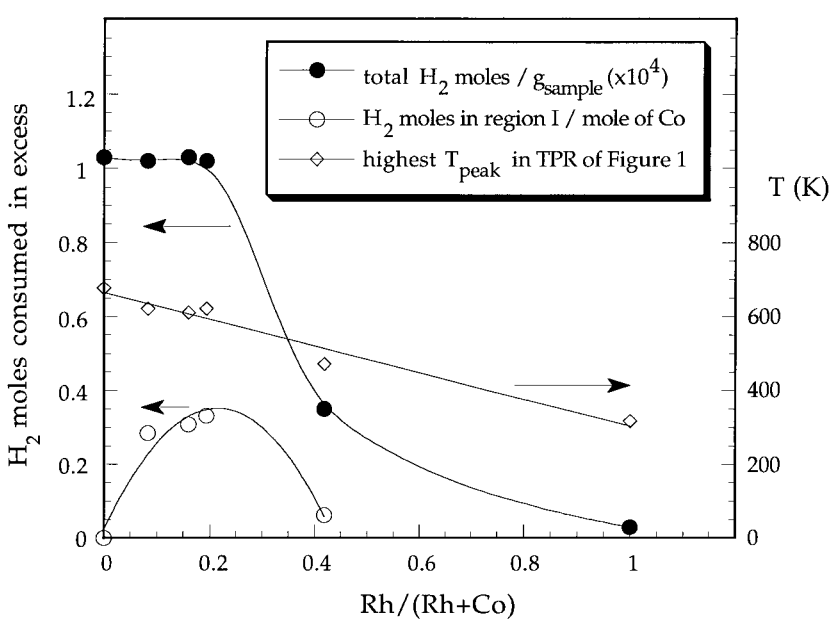


**FIG. 2.** Excess of $H_2$ consumed and temperature of the peak for the highest temperature reduction peak in the TPR experiments on Co–Rh/$Nb_2O_5$ catalysts as functions of the Rh concentration in the catalyst.

noble metal-based bimetallic catalysts. The noble metal serves as a site for $H_2$ dissociative adsorption and a hydrogen storage source to catalyze the reduction of the other metal (in this case, the $Rh_2O_3$ is reduced well before the Co oxide). Similar effects were reported on Co–Pt (67) and Co–Rh (43) bimetallic catalysts, as well as on unsupported bimetallic samples (81). On the other hand, the bimetallic catalysts showed a TPR peak that shifted only from 363 to 419 K as the Rh loading increased. This sharp peak was quite similar in shape and reduction temperature to $Rh_2O_3$ in the monometallic Rh/Nb catalyst (367 K) and in the pure $Rh_2O_3$ sample (408 K) (43). Thus, the addition of Co has no clear influence on the reduction behavior of the $Rh_2O_3$ phase, or at least the influence is not significantly greater than that due to the $Nb_2O_5$ support material. This is consistent with XPS analysis (54), which showed that the $Rh_2O_3$ phase covers the $Co_3O_4$ particles.

According to Table 3, the hydrogen consumption in the TPR of these bimetallic catalysts exceeded the stoichiometric requirements in all samples. However, this excess per mass of sample remained approximately unchanged in the low Rh content samples as shown in Fig. 2. The excess amount of hydrogen decreased for the Co72Rh/Nb sample and was practically zero in the monometallic Rh/Nb. This suggests that the presence of Co is related to the excess in hydrogen consumption in the TPRs. Table 3 shows that the amount in excess for the bimetallic catalysts is mainly concentrated in Region I of the TPR where Rh oxide is reduced. Figure 2 also shows that this excess hydrogen consumed in Region I corresponds closely to the stoichiometric amount of hydrogen needed to reduce $Co_3O_4$ to CoO ($H_2/Co = 0.33$). It is well known that Rh oxide is reduced at near room temperatures to form $Rh^0$, and again we believe this $Rh^0$ catalyzes the reduction of Co oxide (in this case, $Co_3O_4$ to CoO) at a much lower temperature than would occur in the absence of Rh. Similar results were reported on Pt–Co/$Nb_2O_5$ (68) and Pt–Co/$Al_2O_3$ (69). Therefore, the reduction peak detected in the high temperature region can be assigned primarily to the reduction of CoO to $Co^0$, plus another unknown mechanism of excess hydrogen consumption. If this is taken into account, we now notice an excess of hydrogen consumed in Region II that was not clearly shown before. We can here speculate that this excess in the high temperature region is probably due to partial reduction of the support as mentioned above and/or due to hydrogen spillover onto or into the support material. Table 3 shows that the total excess hydrogen consumed in these TPR experiments was on the order of $2–3 \times 10^{14}$ H atoms per $cm^2$ of $Nb_2O_5$ support, if Co is present. This corresponds to about one H for every 2–5 surface oxygen atoms on the $Nb_2O_5$ support (depending on its surface structure). Thus, it could easily correspond to formation of a surface OH species at the Co/$Nb_2O_5$ interface. It is also possible to account for the excess hydrogen by partial reduction of bulk $Nb_2O_5$ or absorption of hydrogen by $Nb_2O_5$. A TPR of pure $Nb_2O_5$ (not shown) resulted in a single reduction peak between 1082 and 1268 K that represented a consumption of $\sim 2.4 \times 10^{14}$ atoms of H per $cm^2$ of $Nb_2O_5$. It seems that the presence of Co decreased the reduction temperature of the $Nb_2O_5$ support.

When the Rh content increases, as for the Co72Rh/Nb sample, the excess of hydrogen consumed in Region I is drastically reduced, becoming almost zero as for the monometallic Rh/Nb sample. Thus, there is no significant excess in Region I to account for the low temperature reduction of Co oxide in the case of the Co72Rh/Nb sample. The excess hydrogen consumption in Region II also decreased. It is clear that the increasing presence of Rh reduces the excess of hydrogen consumed in the reduction of these samples. Perhaps the Rh blocks the role of Co in creating this excess.

### 3.2. *CO Hydrogenation*

Catalytic data of all samples were collected for analysis and comparison by averaging three consecutive injections collected after 24 h, even though steady state was attained after ~8 h on stream. The total CO conversion on the Co/Nb sample and on the bimetallics was between ~19 and 27% after low temperature reduction (LTR) and between ~15 and 24% after high temperature reduction (HTR). The Rh/Nb sample converted ~45% of the total CO in both cases. This extremely high activity was also reported on another Rh/$Nb_2O_5$ catalyst (51).

Figure 3 shows the [$CO_2/H_2O$] ratio produced on all samples. The highest value is smaller than 0.2, suggesting that the formation of hydrocarbons is favored on all samples.

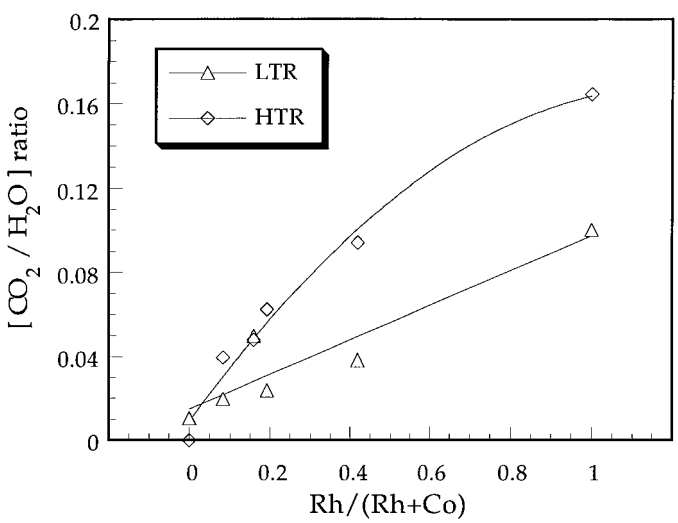


**FIG. 3.** Ratio [$CO_2/H_2O$] produced in the CO hydrogenation reaction (at 423 K and 0.1 MPa, $H_2/CO = 2$) over Co–Rh/$Nb_2O_5$ catalysts, reduced at 573 K (low temperature reduction, LTR) and 773 K (high temperature reduction, HTR), as a function of the Rh concentration in the catalyst.

In addition, the lower [$CO_2/H_2O$] ratio produced on the Co/Nb sample suggests the water–gas shift reaction is not significant on Co-based catalysts, as noted elsewhere (12). The [$CO_2/H_2O$] ratio increases as the Rh content increases, which indicates that the rate of $CO_2$ production increases faster than the rate of $H_2O$, producing reactions as Rh is added to the catalysts. However, the amount of hydrocarbons produced (and also $H_2O$) increased significantly with the presence of Rh as will be discussed later.

The effect of the reduction temperature can be evaluated from several aspects. First of all, we will comment on the reduction time of 2 h applied to the monometallic catalysts. In the case of the Co/Nb sample reduced at LTR, it is very likely that the reduction degree of the Co oxide was low at the beginning of the CO hydrogenation reaction due to the short reduction time and the low reduction temperature. However, after ~8–10 h on stream under the $CO/H_2$ atmosphere, the remaining Co oxide was most likely reduced. For the Rh/Nb sample, the 2-h reduction time was not a problem since Rh oxide is easily reducible even at room temperature as the TPR analysis has already shown.

Figure 4a shows the overall reaction rate as a function of the time-on-stream for the monometallic catalysts. The Co/Nb sample reduced at LTR was quite active (1.26 $\mu$mol CO converted per $g_{cat}$; total CO conversion of 26.9%) in comparison to a 5% $Co/Nb_2O_5$ catalyst of similar BET area and reduced at 573 K (0.65 $\mu$mol CO converted per $g_{cat}$; total CO conversion of 9.7%) (48). Silva *et al.* (48) observed that the reaction rate dropped by a factor of ~6 after reduction at 773 K. Our Co/Nb sample showed a comparable decrease in the reaction rate by a factor of ~7 after HTR. Soares *et al.* (68) also obtained a decrease in the reaction rate by a factor similar to ours after reduction at 573 and 773 K on another 5% $Co/Nb_2O_5$ catalyst. The reaction rate on the Rh/Nb sample reduced at LTR also dropped after HTR, however by a lower degree (from 3.0 to 2.09 $\mu$mol CO converted per $g_{cat}$). In general, this decrease in the reaction rate after reduction at high temperature is attributed to the so-called metal–support interaction phenomena that is likely to occur when dealing with reducible support material such as $Nb_2O_5$ (48, 64). The higher reduction temperature promotes migration of support species onto the active centers on the surface of the catalyst that get blocked by those patches of support originated material, thus causing the activity decay (48). The Co/Nb and Rh/Nb samples reduced at HTR were also reoxidized after the CO hydrogenation reaction by a 5% $O_2/N_2$ mixture at 673 K. These samples were then reduced at LTR for comparison with the same samples freshly reduced at LTR (Fig. 4a). It was observed that the reaction rate on Co/Nb was only partially recovered (~50%), being in accordance with Silva *et al.* (48). However, this deactivation process seems to be irreversible for the Rh/Nb sample, and this agrees with Kunimori *et al.* (71). On the other hand, the overall reaction rate of the bimetallic samples reduced at LTR and that of those reduced at HTR did not vary considerably (see Fig. 4b), suggesting that the combination of Co and Rh somehow suppressed the deactivation resulting from metal–support interactions. This observation also occurred in other bimetallic catalysts supported on $Nb_2O_5$ (68, 72). Figure 5a summarizes the effects of the Rh content and the reduction temperature on the steady-state rate of CO hydrogenation.

Table 4 presents the active metal dispersions determined by hydrogen chemisorption measurements (which were

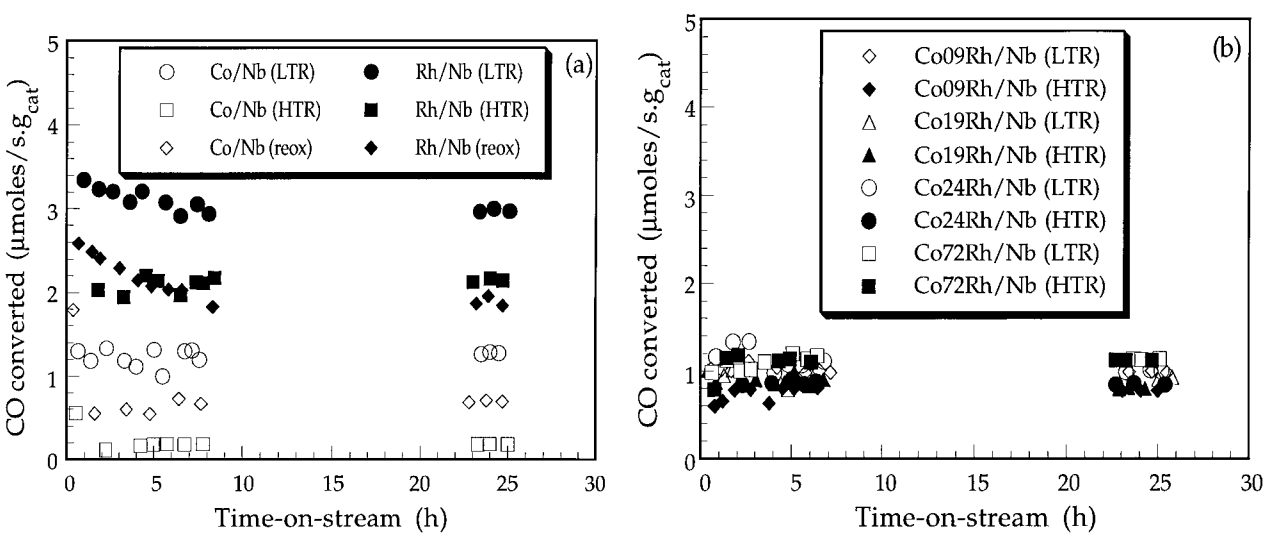


**FIG. 4.** Rate of CO hydrogenation (at 423 K and 0.1 MPa, $H_2/CO = 2$) over Co- and Rh-based catalysts supported on $Nb_2O_5$, reduced at 573 K (low temperature reduction, LTR) and 773 K (high temperature reduction, HTR), as a function of the time-on-stream. Monometallic catalysts reduced at HTR were reoxidized and rereduced at LTR (named *reox* samples). (a) Monometallic catalysts $Co/Nb_2O_5$ and $Rh/Nb_2O_5$. (b) Bimetallic catalysts Co–Rh/$Nb_2O_5$.

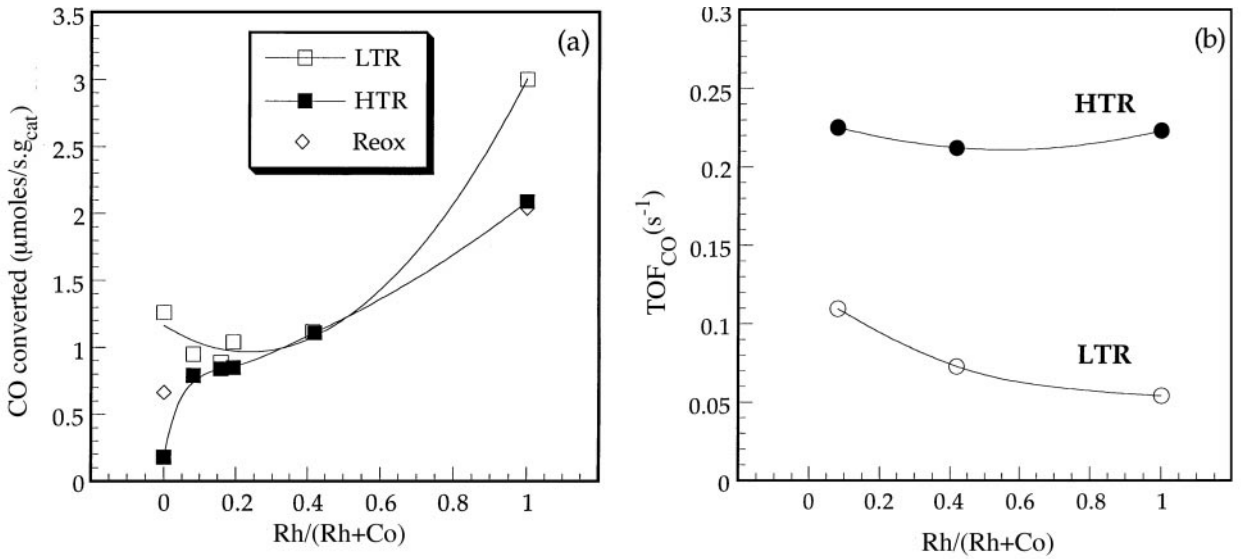


**FIG. 5.** Steady-state rate of CO hydrogenation (at 423 K and 0.1 MPa, $H_2/CO = 2$, 23–25 h on stream) over Co- and Rh-based catalysts supported on $Nb_2O_5$, reduced at 573 K (low temperature reduction, LTR) and 773 K (high temperature reduction, HTR), as a function of the Rh concentration in the catalyst. Monometallic catalysts reduced at HTR were reoxidized and rereduced at LTR (named *reox* samples). (a) Rates per gram of catalyst. (b) Rates per active site (number of active sites obtained from irreversible hydrogen adsorption measurement).

made only on some of the catalysts), assuming that each surface active metal atom adsorbs one H atom. Since the support can reversibly adsorb hydrogen at 298 K, the irreversibly adsorbed H amount is thought to provide a better measure of the active metal area. Listed also in Table 4 is the fraction of the BET surface area that is active metal, as determined by this irreversible hydrogen adsorption. The dispersion values in Table 4 provide a crude estimate of the active metal surface area, but may be missing the Co area as suggested by Bartholomew *et al.* (82, 83) due to activated adsorption of $H_2$ on Co particles (chemisorption may be too reversible and too slow to reach equilibrium). Since Rh is known to activate $H_2$ at room temperature, we expect that H spills over to the Co sites in the bimetallics (as our TPR analysis suggested above), so this method would probably only be a problem for the Rh-free Co catalyst, for which we do not present H adsorption data anyway.

**TABLE 4**

**Surface Coverage on Co–Rh/$Nb_2O_5$ Catalysts**

| | $H_{total}/M^a$ | | $H_{irrev}/M^a$ | | $S_M^H/BET^b$ | | |
|---|---|---|---|---|---|---|---|
| Catalyst | LTR | HTR | LTR | HTR | LTR | HTR | $S_M^{XPS}/BET^c$ |
| Rh/Nb | 1.39 | 0.76 | 0.67 | 0.11 | 0.12 | 0.019 | 0.015 |
| Co72Rh/Nb | 0.18 | 0.097 | 0.029 | 0.010 | 0.046 | 0.016 | 0.044 |
| Co24Rh/Nb | N/A | N/A | N/A | N/A | N/A | N/A | 0.027 |
| Co19Rh/Nb | N/A | N/A | N/A | N/A | N/A | N/A | 0.031 |
| Co09Rh/Nb | 0.15 | 0.14 | 0.024 | 0.009 | 0.024 | 0.010 | 0.034 |
| Co/Nb | N/A | N/A | N/A | N/A | N/A | N/A | 0.013 |

[a] Ratio of the number of H atoms adsorbed to the total number of metal sites (from continuous-flow $H_2$ adsorption at room temperature).

[b] Ratio of the active metal surface area for irreversible H adsorption (assuming $10^{19}$ H atoms/$m^2$) to the total BET surface area of the catalyst.

[c] Fraction of $Nb_2O_5$ total surface area covered by $Rh_2O_3/Co_3O_4$ islands on the catalysts in their calcined form as determined by XPS (54).

Figure 5b presents the corresponding CO turnover frequencies (TOFs) calculated from the steady-state rates per gram presented in Figs. 4 and 5a using the irreversible hydrogen adsorption measurements of Table 4 to estimate the number of active metal surface sites. As can be seen, the TOFs for the catalysts are nearly independent of Rh content. However, the apparent TOFs for the catalysts treated with HTR are two to three times higher than those treated only with LTR. One must be cautious when presenting reaction rates per active site for catalysts in the SMSI state, because the active surface area available may be quite complex and may change during reaction in the presence of reaction products, as already stated elsewhere (48, 70).

Our XPS data from a previously published XPS analysis of these same catalysts in their calcined form (54) showed that rather thick $Co_3O_4$ islands existed on 2.7–4.4% of the support surface (provided that *both* Rh *and* Co were present) and that these islands were themselves covered with a Rh oxide layer of variable thickness (depending on the Rh content). In between these islands was a submonolayer, fully dispersed $Co^{2+}$ species. In Table 4 we also list the fractions of the BET surface areas of the calcined catalysts that are covered by these $Rh_2O_3/Co_3O_4$ islands, as determined by XPS in (54). Interestingly, the irreversible H adsorption measurements on the Rh + Co catalysts of Table 4 indicate that almost the same fraction of the total BET area (i.e., 2.4–4.6%) is active metal islands after

**TABLE 5**

**CO Hydrogenation Selectivity (Mol% of Carbon Reacted)[a]**

| | Catalysts | | | | | | | | | | | |
|---|---|---|---|---|---|---|---|---|---|---|---|---|
| | Co/Nb | | Co09Rh/Nb | | Co19Rh/Nb | | Co24Rh/Nb | | Co72Rh/Nb | | Rh/Nb | |
| Products | LTR | HTR | LTR | HTR | LTR | HTR | LTR | HTR | LTR | HTR | LTR | HTR |
| $CO_2$ | 0.37 | 0 | 0.69 | 0.86 | 1.76 | 1.33 | 2.19 | 1.11 | 1.72 | 5.85 | 6.13 | 9.41 |
| $CH_4$ | 65.16 | 48.10 | 26.51 | 17.15 | 23.49 | 15.09 | 22.99 | 14.89 | 20.15 | 11.86 | 27.89 | 26.46 |
| $C_{2-4}$ | 29.89 | 51.90 | 26.42 | 14.08 | 20.53 | 12.43 | 19.03 | 11.74 | 13.17 | 9.34 | 22.62 | 24.01 |
| $C_{5-12}$ | 4.58 | — | 16.19 | 20.42 | 15.52 | 13.22 | 14.77 | 13.51 | 17.89 | 10.26 | 8.04 | 9.78 |
| $C^{=}_{5-12}$ | — | — | — | — | — | — | — | — | — | — | 11.17 | 12.23 |
| $C_{13-18}$ | — | — | 14.89 | 30.44 | 22.59 | 48.85 | 26.07 | 49.53 | 23.39 | 55.56 | 12.11 | 10.33 |
| $C^{=}_{13-18}$ | — | — | — | — | — | — | — | — | — | — | 0.70 | 0.76 |
| $C_{19+}$ | — | — | 6.36 | 11.40 | 13.74 | 5.03 | 13.08 | 5.60 | 21.77 | 5.46 | 6.56 | 2.28 |
| $C_2$-OH | — | — | 3.53 | 3.65 | 1.21 | 2.34 | 0.87 | 2.12 | 1.32 | 1.19 | 2.37 | 1.08 |
| *i*-$C_3$-OH | — | — | — | — | — | — | — | — | — | — | 1.30 | 1.70 |
| $C_3$-OH | — | — | 5.41 | 2.00 | 1.16 | 1.71 | 1.00 | 1.50 | 0.59 | 0.48 | 0.60 | 0.89 |
| $C_4$-OH | — | — | — | — | — | — | — | — | — | — | 0.51 | 1.07 |
| Total | 100 | 100 | 100 | 100 | 100 | 100 | 100 | 100 | 100 | 100 | 100 | 100 |
| $C^{=}_4$/*n*-$C_4$ | 0.27 | — | 0.97 | 1.03 | 0.76 | 1.25 | 1.47 | 2.19 | 1.53 | 4.31 | 1.56 | 2.12 |

[a] The symbol "=" refers to olefins.

LTR as was covered by these $Rh_2O_3/Co_3O_4$ islands in the calcined catalysts (~3–4.4%). This suggests that the calcined Rh + Co islands maintain almost their same surface area upon low temperature reduction and that only they (and not the dispersed Co species) are active with respect to irreversible H adsorption. These XPS measurements in Table 4 show that the island area fraction was nearly constant (within the range 2.7–4.4%) for all four Rh + Co mixed catalysts (i.e., for Rh/Co ratios of 0.09, 0.19, 0.24, and 0.72). This gives one confidence that the lack of dependence upon Rh content displayed by the TOFs in Fig. 5b is true for *all four* Rh + Co compositions, even though we could show TOFs in Fig. 5b only for the two mixed compositions for which we measured H chemisorption. Furthermore, this lack of dependence of TOF upon Rh content may to some extent be explained by the fact that the XPS showed that the topmost atomic layers of these Rh + Co islands were nearly pure Rh (i.e., with no or little Co), at least in their calcined form. It appears in Table 4 that the addition of Co inhibited the dramatic gain of metal surface area seen upon low temperature reduction for the calcined Rh/Nb catalyst. This very high dispersion seen for the pure Rh/Nb catalyst helps explain its more dramatic loss of active metal area upon HTR: the higher initial dispersion renders it more susceptible to Rh decoration by support species or to sintering during HTR.

Figure 5b shows that the TOF on the bimetallic and the pure Rh/Nb catalysts increased after HTR. Since the number of reacted CO molecules per gram of catalyst did not vary considerably from LTR to HTR (Fig. 5a), the decrease in active surface area after HTR (and consequently, the decrease in metal dispersion) is the main reason that the TOF appears to increase after HTR. Generally in the CO hydrogenation reaction, catalysts in the SMSI state (i.e., after HTR) show higher activity and higher selectivity to long chain hydrocarbons, compared to catalysts in the non-SMSI state (i.e., after LTR only) (84). This is in agreement with our results (see Table 5 below for the hydrocarbon selectivities). Enhanced activity in CO hydrogenation was also observed in Ni/$Nb_2O_5$ or Ni/$TiO_2$ after HTR (52). For a Rh/$Nb_2O_5$ catalyst, it was suggested that the activity increase in the CO hydrogenation reaction was caused by mild decoration of Rh metal by support species like $NbO_x$ (85). These species, associated with Rh, enhanced CO dissociation further. However, when the level of decoration was significantly increased, the Rh sites were completely hindered by those support species, then become inaccessible to chemisorption, and, consequently, to catalysis. A similar conclusion was earlier reported on a Rh/$TiO_2$ catalyst (73).

Table 5 and Fig. 6 present product selectivities based on the moles of carbon reacted after 24 h on stream for the range of observed products. Note that $CH_4$, $C_{2-4}$, $C_{5-12}$, $C_{13-18}$, and $C_{19+}$ correspond to saturated hydrocarbons with the carbon subscript being the number of carbon atoms in the chain. The range $C_{2-4}$ may also contain some $C_{2-4}$ olefins (ethene and propene) that were not resolved from the more pronounced saturated hydrocarbon chromatographic peaks. However, no unsaturated, low-molecular-weight hydrocarbons were detected on the TCD chromatograph, suggesting that the production of these olefins is negligible. Olefins $C^{=}_4$ (butenes) were well resolved and detected on most of the samples. Higher molecular weight olefins ($C^{=}_{5-12}$ and $C^{=}_{13-18}$) were detected on the Rh/Nb catalyst only. Alcohols $C_2$–OH (ethanol) and $C_3$–OH (propanol) were also

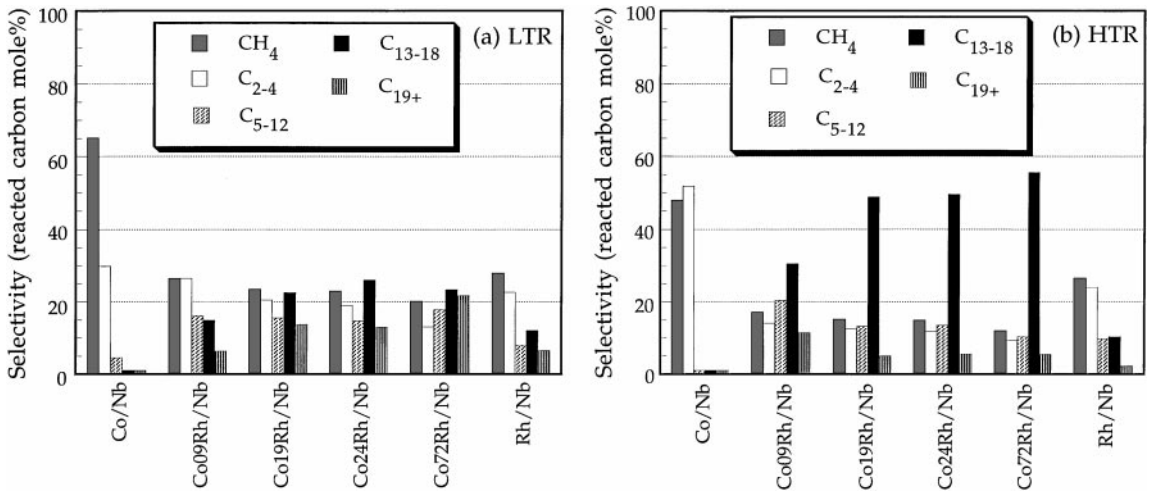


**FIG. 6.** Hydrocarbon selectivities (based on mol% of C reacted) for the steady-state CO hydrogenation reaction (at 423 K and 0.1 MPa, $H_2/CO = 2$) as a function of the catalyst sample. (a) Catalysts reduced at 573 K (low temperature reduction, LTR). (b) Catalysts reduced at 773 K (high temperature reduction, HTR).

detected on most of the samples, but only the Rh/Nb catalyst produced some i-$C_3$–OH (isopropanol) and $C_4$–OH (butanol).

It can be seen in Table 5 and Fig. 6 that the product selectivity of the Co/Nb catalyst reduced at 573 K (LTR) was comparable to the 5% $Co/Nb_2O_5$ catalyst reduced at 573 K of Silva *et al.* (48). After reduction at 773 K, they observed a considerable increase in the selectivity toward high-molecular-weight hydrocarbons $C_{5+}$ from 16.1 to 48.8% with a correspondent drop in methane selectivity from 54.3 to 14.1%. Our Co/Nb catalyst reduced at HTR showed a less pronounced decrease in methane selectivity from 65.1 to 48.1% (48). In addition, we did not detect appreciable amounts of products heavier than *n*-butane on the Co/Nb catalyst reduced at HTR. Silva *et al.* (48) have suggested, after high temperature reduction, that $NbO_x$ species originating from the support material were responsible for creating new sites active for carbon chain growth and increased the formation of high-molecular-weight hydrocarbons. The 2% Co content of our Co/Nb catalyst, after reduction at HTR, may create stronger support interactions with the active phase due to its smaller crystallites compared to the crystallites present in the 5% catalyst of Silva *et al.* (48), as previously discussed in the TPR analysis. In this case, this interaction could reach a level that the promoting effect of the $C_{5+}$ hydrocarbons could not since the new active sites may be inaccessible or not even be created. Indeed, Levin *et al.* (73) have suggested a similar explanation for a $Rh/TiO_2$ catalyst. In their report, it was observed that the presence of $TiO_x$ species promoted methane formation from CO hydrogenation when the surface fraction covered by those species was smaller than ~20%. However, the catalyst was practically inactive when that fraction reached ~40%. Therefore, it is suggested that, under mild conditions, the metal–support interaction promotes the selectivity of a specific range of products in the CO hydrogenation. However, high concentrations of support-originating species on the surface behave just like a catalyst poisoning agent (74). Furthermore, the low Co content of 2% of our Co/Nb catalyst may limit its activity for producing $C_{5+}$ hydrocarbons. A 1% $Co/Al_2O_3$ catalyst (75) was practically inactive in the CO hydrogenation reaction after reduction at 673 K. Lee and Bartholomew (76) have suggested that support-originating species preferentially block the access to small Co crystallites. Table 5 and Fig. 6 also show that the Rh/Nb catalyst presented a quite diversified and an uncommon product distribution for a Rh-based catalyst. Among the products, we detected high-molecular-weight olefins, alcohols from ethanol to butanol, and saturated hydrocarbons from 1 to 27 carbon atoms in the chain. Iizuka *et al.* (51) also observed a considerable amount of heavy hydrocarbons produced from CO hydrogenation on a $Rh/Nb_2O_5$ catalyst.

The product distributions of our bimetallic catalysts from the CO hydrogenation reaction clearly showed a significant change upon the addition of Rh to Co as opposed to the study of Van't Blik (43) who did not observe a significant difference for Co–Rh on $Al_2O_3$ or $TiO_2$ in the $CO/H_2$ reaction at 523 K and 1 atm with $[H_2/CO] = 3$. Their selectivities toward methane and $C_{4+}$ hydrocarbons were ~50–70% and ~10–25% respectively, consistent with their higher reaction temperature and higher $H_2/CO$ ratio which would favor methanation and disfavor the formation of long chain hydrocarbons. In addition, Van't Blik (43) did not observe a noticeable change in product distribution after reduction of their Co–Rh bimetallics at 773 K compared to the reduction at 523 K. Our Co–Rh bimetallics presented a significant alteration of the product selectivities compared to the monometallic Co/Nb. In Table 5, the selectivity toward

methane dropped from 65% on the Co/Nb to 20–27% on the bimetallics, depending on the Rh content. The selectivity toward lighter hydrocarbons in the $C_{2\text{-}4}$ range also dropped for the bimetallics compared to Co/Nb. A considerable increase in the selectivity in the gasoline range ($C_{5\text{-}12}$) was observed, changing from ~5% on the Co/Nb to 13–20% on the bimetallics. However, the most significant effect occurred in the heavier product range, diesel ($C_{13\text{-}18}$) and $C_{19+}$, plus the oxygenated compounds (ethanol and propanol).

Increasing the Rh content of our HTR bimetallic catalysts gives a pronounced promotion of the selectivity toward long chain hydrocarbons, specifically in the diesel range. The diesel range selectivity increased from zero on the Co/Nb to 14–25% on the LTR bimetallics and 31–56% on the HTR bimetallics. (Figure 6 clearly shows that the selectivity toward heavy hydrocarbons, mainly in diesel range, goes through a maximum of around 56% for the Co72Rh/Nb HTR catalysts.) An increase in the selectivity toward heavy hydrocarbons was also obtained by Silva *et al.* (48) for a 5% Co/$Nb_2O_5$ catalyst after reduction at 773 K. In that work, this effect was attributed to the formation of new active sites from metal–support interactions as discussed earlier. However, the lower Co content and the lower mass of sample tested here suggest that the formation of special species originating from the support were not entirely responsible for the production of heavy hydrocarbons, but also a bimetallic effect must be involved. (For example, in Table 5 and Fig. 6, it is observed that the Co/Nb catalyst was practically inactive for long carbon chain hydrocarbons formation.) Increased selectivity for heavy hydrocarbons was also detected on other bimetallic catalysts such as Fe–Co, Co–Ni, and Ni–Fe in the CO hydrogenation reaction at 523 K and 10 atm (77). Iglesia *et al.* (31) obtained $C_{5+}$ hydrocarbons selectivities in the range of 85–91% on Co–Ru/$TiO_2$ catalysts.

The bar diagrams in Fig. 6 clearly point out that the selectivity toward methane and $C_{2\text{-}4}$ hydrocarbons for the bimetallics did not vary markedly with increasing Rh content. This is reminiscent of the fact that the total TOF for CO conversion was nearly independent of Rh content in these bimetallics (Fig. 5b). We suggested above that this may be due to the topmost atomic layers of the Rh + Co islands being nearly pure Rh (as shown by XPS in their calcined state). This may also explain the constancy in selectivity for these less demanding products. Note that the methane formation rate on the pure Co catalyst after LTR is ~threefold higher than on the bimetallic catalysts, which have methane formation rates comparable to those of the pure Rh catalysts.

Olefins, except $C_4^=$, were not detected on the Co-containing catalysts. The $C_4^=$ content increased relative to butane on the bimetallics, compared to the Co/Nb catalyst (last line in Table 4). In contrast, the Rh/Nb catalyst was active for the formation of long chain olefins $C_{5\text{-}12}^=$ and $C_{13\text{-}18}^=$. Villeger *et al.* (45) had already shown that the addition of Rh to Co catalysts results in increased selectivities toward $C_2^=$ and $C_3^=$ in the CO hydrogenation reaction. However, these olefins were not detected in the present study.

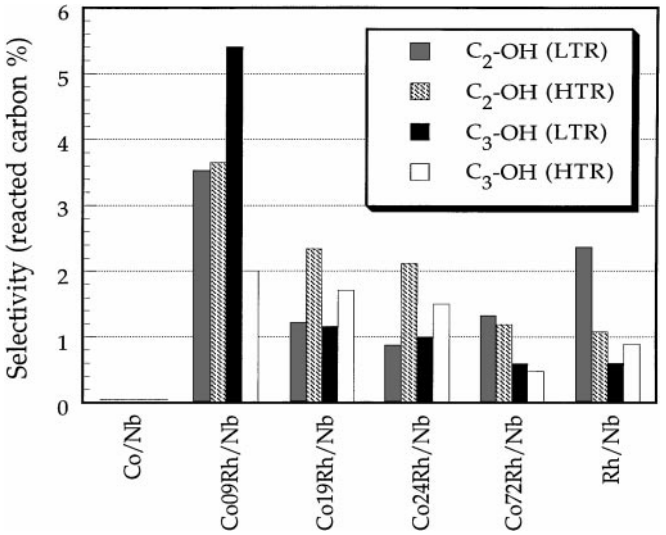


**FIG. 7.** Ethanol and propanol selectivities (based on mol% of C reacted) for the steady-state CO hydrogenation reaction (at 423 K and 0.1 MPa, $H_2/CO = 2$) as a function of the catalyst sample, reduced at 573 K (low temperature reduction, LTR) and 773 K (high temperature reduction, HTR).

Figure 7 shows that alcohol selectivity increased as the Rh content in the bimetallics decreased. Alcohols were not detected on the Co/Nb, but selectivities of 0.9–3.5% and 0.6–5.5% for ethanol and propanol, respectively, were obtained on the bimetallic catalysts, depending on the Rh content. Therefore, the presence of Rh is necessary for the formation of these alcohols. The lower Rh content bimetallic Co09Rh/Nb produced the highest selectivities toward ethanol (~3.5%) and propanol (~5.5%) among the catalysts tested after LTR. This increase in selectivity for ethanol and propanol was also reported by Ladner and Richards (29) for the Co-Rh/$TiO_2$ system, with selectivities of 13–18%. However, the authors performed the CO/$H_2$ reaction at a total pressure of 100 atm, thermodynamically favoring alcohol formation. XPS analysis (54) revealed that the calcined Co09Rh/Nb catalyst has a thin Rh oxide surface overlayer, approximately two times thicker than a monolayer, which may be responsible for promoting the selectivity to alcohol formation.

Also interesting is the fact that we did not detect formation of methanol on these catalysts. It is common knowledge that under the reaction conditions used in this study, the thermodynamics of methanol formation from CO hydrogenation is not favored (78). Lee *et al.* (79) suggested that the presence of $Rh^{n+}$ favors methanol production, while

$Rh^0$ is related to the formation of ethanol. The TPR results clearly indicate that, at the reduction temperatures used (LTR and HTR), most rhodium should be reduced to $Rh^0$. Therefore, our catalytic results for ethanol formation are consistent with those of Lee *et al.* (79).

## 4. CONCLUSIONS

Our results show the synergistic effect of bimetallic catalysts and the promoter effect of a noble metal. This synergy suggests that Co and Rh particles must be in intimate contact, consistent with the surface structure of the calcined precursors of these Co–Rh/$Nb_2O_5$ catalysts (54). The increased formation of long chain hydrocarbons by the bimetallics compared to the Rh/Nb catalyst indicates that Rh is taking advantage of the carbon chain growth features of Co-containing catalysts in the CO hydrogenation reaction. The low Co content on the catalysts was most effective when Rh was present, probably because Co reducibility was facilitated as TPR analysis indicated. Of the bimetallic catalysts, the one with the lowest Rh content produced the highest alcohol yields. The combination of Co and Rh has significantly inhibited the catalyst deactivation caused by metal–support interaction after reduction at high temperatures. The total CO hydrogenation reaction rate and the selectivity for methane were approximately constant as the Rh concentration on the bimetallics increased, suggesting that the specific surface area of active metal (Rh + Co) precursor oxide did not vary significantly as the Rh concentration increased on these catalysts. This result agrees with hydrogen adsorption measurements on the bimetallic catalysts and with the XPS surface structural characterization of the calcined Co–Rh/$Nb_2O_5$ catalysts.

## ACKNOWLEDGMENTS

The authors thank the technical assistance of Mr. Antônio José de Almeida with the catalytic tests. Financial support for this research by CNPq (Conselho Nacional de Desenvolvimento Científico e Tecnológico) and FINEP (Financiadora de Estudos e Projetos) is gratefully acknowledged by A.F. and M.S. C.T.C. acknowledges the DOE-BES Chemical Sciences Division as well as the National Science Foundation Division of International Programs for partial support of this work.

## REFERENCES

1. Lee, G. v. d., and Ponec, V., *Catal. Rev. Sci. Eng.* **29**(2-3), 183 (1977).
2. Burch, R., and Petch, M. I., *Appl. Catal.* **88**, 39 (1992).
3. Bhasin, M. M., and O'Connor, G. L., Belgian patent 824822, 1975.
4. Bhasin, M. M., Belgian patent 824823, 1975.
5. Bhasin, M. M., Bartley, W. J., Ellgen, P. C., and Wilson, T. P., *J. Catal.* **54**, 120 (1978).
6. The Research Association for $C_1$ Chemistry, "Progress in $C_1$ Chemistry in Japan." Kodansha, Tokyo, 1989.
7. Herman, R. G., *Stud. Surf. Sci. Catal.* **64**, 265 (1991).
8. Ichikawa, M., *Bull. Chem. Soc. Jpn.* **51**, 2268 (1978).
9. Ichikawa, M., *Bull. Chem. Soc. Jpn.* **51**, 2273 (1978).
10. Ichikawa, M., *Chemtech* **674** (1982).
11. Kawai, M., Uda, M., and Ichikawa, M., *J. Phys. Chem.* **89**, 1654 (1985).
12. Anderson, R. B., "The Fischer-Tröpsch Synthesis." Academic Press, Orlando, 1984.
13. Hachenberg, H., Wunder, F., Leupoid, E. I., and Schmidt, H. J., Eur. patent application 21330, 1981.
14. Kuznetsov, V. L., Lisitsyn, A. S., Golovin, A. V., Aleksandrov, M. N., and Yermakov, Yu. I., *in* "Homogeneous and Heterogeneous Catalysis" (Yu. I. Yermakov and V. Likholobov, Eds.). VNU Science Press, Utrecht, The Netherlands, 1986.
15. Lisitsyn, A. S., Golovin, A. V., Chuvilin, A. L., Kuznetsov, V. L., Romanenko, A. V., Danilyuk, A. F., and Yermakov, Yu. I., *Appl. Catal.* **55**, 235 (1989).
16. Fujimoto, K., and Oba, T., *Appl. Catal.* **51**, 289 (1985).
17. Derule, H., Blanchard, M., and Canesson, P., *Appl. Catal.* **50**, L1 (1989).
18. Sinfelt, J. H., "Bimetallics Catalysts—Discoveries, Concepts and Applications." Wiley, New York. 1983.
19. Schwank, J., *Stud. Surf. Sci. Catal.* **64**, 225 (1991).
20. Courty, P., Durand, D., Fruend, E., and Sugier, A., *J. Mol. Catal.* **17**, 241 (1982).
21. Baker, J. E., Burch, R., and Golunski, S. E., *Appl. Catal.* **53**, 279 (1989).
22. Elliot, D. J., and Pennella, F., *J. Catal.* **102**, 464 (1986).
23. Mouaddib, N., and Perrichon, V., "Proc. 9th International Congress on Catalysis, Calgory, 1988" (H. J. Phillips and M. Ternan, Eds.). Chem Institute of Canada, Ottawa, 1988.
24. Kintaichi, Y., Kuwahara, Y., Hamada, H., Ito, T., and Wakabayashi, J., *Chem. Lett.* **1305** (1985).
25. Guczi, L., Matusek, K., Bogyai, I., Garin, F., Puges, P. E., Girard, P., and Maire, G., *Mol. Chem.* **1**, 335 (1986).
26. Guczi, L., Hoffer, T., Zsoldos, Z., Zyade, S., Maire, G., and Garin, F., *J. Phys. Chem.* **95**, 802 (1991).
27. Fukuoka, A., Xiao, F. S., Ichikawa, M., Shriver, D. F., and Hendeson, W., *Shokubai* **32**, 368 (1990).
28. Yin, Y.-G., Zhang, Z., and Sachtler, W. M. H., *J. Catal.* **138**, 721 (1992).
29. Ladner, W. R., and Richards, D. G., "International Congress on Coal Science." Pergamon, Sydney, Australia, 1985.
30. Matsuzaki, T., Takeuchi, K., Hanaoka, T., Arakawa, H., and Sugi, Y., *Appl. Catal. A* **105**, 159 (1993).
31. Iglesia, E., Soled, S. L., Fiato, A., and Via, G. H., *J. Catal.* **143**, 345 (1993).
32. Iglesia, E., Reyes, S. C., and Madon, R. J., *J. Catal.* **129**, 238 (1991).
33. Madon, R. J., Iglesia, E., and Reyes, S. C., *J. Phys. Chem.* **95**, 7795 (1991).
34. Iglesia, E., Reyes, S. C., and Soled, S. L., *in* "Computer Aided Design of Catalysts" (E. R. Becker and C. J. Pereira, Eds.). Dekker, New York, 1992.
35. Iglesia, E., Reyes, S. C., Soled, S. L., and Madon, R. J., *in* "Advances in Catalysis and Related Subjects" (D. D. Eley, P. B. Weisz, and H. Pines, Eds.), Vol. 39, p. 221. Academic Press, San Diego, 1993.
36. Iglesia, E., Soled, S. L., and Fiato, R. A., *J. Catal.* **137**, 212 (1993).
37. Beuther, H., Kibby, C. L., Kobylinski, T. P., and Pannell, R. B., U.S. patent 4,413,064, Gulf Research and Development Co., 1983.
38. Beuther, H., Kibby, C. L., Kobylinski, T. P., and Pannell, R. B., U.S, patent 4,493,905, Gulf Research and Development Co., 1985.
39. Beuther, H., Kobylinski, T. P., Kibby, C. L., and Pannell, R. B., U.S. patent 4,585,798, Gulf Research and Development Co., 1986.
40. Kobylinski, T. P., Kibby, C. L., Pannell, R. B., and Eddy, E. L., U.S. patent 4,605,676, Chevron Research Co., 1986.
41. Knifton, J. F., and Lin, J. J., U.S. patent 4,366,259, Texaco, Inc., 1982.
42. Goodwin, J. G., Jr., "Symposium on Methane Upgrading." ACS, Atlanta, 1991.
43. Van't Blik, H. J. F., Ph.D. thesis, Univ. of Technology, Eindhoven, Holland, 1984.
44. Ichikawa, M., *J. Catal.* **56**, 127 (1979).

45. Villeger, P., Barrault, J., Barbier, J., Leclerq, G., and Maurel, R., *Bull. Soc. Chim. Fr.* **I-413** (1979).
46. Forzatti, P., Tronconi, E., and Pasquon, I., *Catal. Rev. Sci. Eng.* **32**(4), 279 (1991).
47. Macedo, J. C. D., Schmal, M., and Dalmon, J. A., *in* "Proceedings of the X Symposium Iberoamerican on Catalysis," Vol. 2, p. 666. 1986.
48. Silva, R. R. C. M., Schmal, M., Frety, R., and Dalmon, J. A., *J. Chem. Soc. Faraday Trans.* **89**(21), 3975 (1993).
49. Frydman, A., Soares, R. R., and Schmal, M., *Stud. Surf. Sci. Catal.* **75**, 2796 (1993).
50. Soares, R. R., Frydman, A., and Schmal, M., *Catal. Today* **16**, 361 (1993).
51. Iizuka, T., Tanaka, Y., and Tanabe, K., *J. Mol. Catal.* **17**, 381 (1982).
52. Vannice, M. A., and Garten, R. L., *J. Catal.* **56**, 236 (1979).
53. Ko, E. I., and Hupp, M., *J. Catal.* **86**, 315 (1984).
54. Frydman, A., Castner, D. G., Schmal, M., and Campbell, C. T., *J. Catal.* **152**, 164 (1995).
55. Ko, E. I., and Weissman, J. G., *J. Catal.* **8**, 27 (1990).
56. Porto, L. M., Master thesis, COPPE/UFRJ and UFSC, Brazil, 1987.
57. "Supelco Gas Chromatography Catalog," p. 713. 1994.
58. Dietz, W. A., *J. Gas Chromatogr.* **February**, 68 (1967).
59. Greenwood, N. N., and Earnshaw, A., "Chemistry of The Elements," p. 1290. Pergamon Oxford, 1984.
60. Arnoldy, P., and Moulijn, J. A., *J. Catal.* **93**, 38 (1985).
61. Brown, R., Cooper, M. E., and Whan, D. A., *Appl. Catal.* **3**, 177 (1982).
62. Paryjczak, T., Rynkowski, J., and Karski, S., *J. Chromatogr.* **188**, 254 (1980).
63. Castner, D. G., Watson, P. R., and Chan, I. Y., *J. Phys. Chem.* **94**, 819 (1990).
64. Silva, R. R. C. M., D.Sc. thesis, COPPE/UFRJ, Rio de Janeiro, Brazil, 1992.
65. Soares, R. R., M.Sc. thesis, COPPE/UFRJ, Rio de Janeiro, Brazil, 1994.
66. Noronha, F. B., D.Sc. thesis, COPPE/UFRJ, Rio de Janeiro, Brazil, 1994.
67. Stranick, M. A., Houalla, M., and Hercules, D. M., *J. Catal.* **103**, 151 (1987); *J. Catal.* **106**, 362 (1987); *J. Catal.* **125**, 214 (1990).
68. Soares, R. R., Aranda, D. A. G., Almeida, A. J., and Schmal, M., "XII Congress Iberoamericano de Catálise." Santiago, Chile, 1994.
69. Zsoldos, Z., Hoffer, T., and Guczi, L., *J. Phys. Chem.* **95**, 798 (1991).
70. Haller, G. L., and Resasco, D. E., *Adv. Catal.* **36**, 173 (1989).
71. Kunimori, K., Abe, H., Yamaguchi, E., Matsui, S., and Uchijima, T., *in* "Proceedings, 8th International Congress on Catalysis, Berlin, 1984." Dechema, Frankfurt-am-Main, 1984.
72. Noronha, F. B., Schmal, M., Primet, M., and Frety, R., *Appl. Catal.* **78**, 125 (1991).
73. Levin, M., Salmeron, M., Bell, A. T., and Somorjai, G. A., *Faraday Symp. Chem. Soc.* (1986).
74. Burch, R., *in* "Hydrogen Effects in Catalysis" (P. Paál and P. G. Menon, Eds.). Dekker, New York, 1988.
75. Reuel, R. C., and Bartholomew, C. H., *J. Catal.* **85**, 78 (1988).
76. Lee, W. H., and Bartholomew, C. H., "Spring Meeting of The California Catalysis Society." Richmond, CA, 1986.
77. Ishihara, T., Eguchi, K., and Arai, H., *Appl. Catal.* **30**, 225 (1987).
78. Storch, H. H., Golumbic, N., and Anderson, R. B., "The Fischer–Tröpsch and Related Synthesis." Wiley, New York, 1951.
79. Lee, G. v. d., Schuller, B., Post, H., Favre, T. L. F., and Ponec, V., *J. Catal.* **98**, 522 (1986).
80. Efstathiou, A. G., Tan, B. J., and Suib, S. L., *J. Catal.* **140**, 564 (1993).
81. Campbell, C. T. C., *Annu. Rev. Phys. Chem.* **41**, 775 (1990).
82. Zowtiak, J. M., and Bartholomew, C. H., *J. Catal.* **83**, 107 (1983).
83. Reuel, R. C., and Bartholomew, C. H., *J. Catal.* **85**, 63 (1984).
84. Bond, G. C., and Burch, R., *Catalysis* **6**, 27 (1983).
85. Hu, Z., Nakamura, H., Kunimori, K., Asano, H., and Uchijima, T., *J. Catal.* **112**, 478 (1988).